Oxidative desulfurization of diesel fuel catalyzed by polyoxometalate immobilized on phosphazene-functionalized silica

Michael Craven[a], Dong Xiao[a,c], Casper Kunstmann-Olsen[a], Elena F. Kozhevnikova[a], Frédéric Blanc[a,b], Alexander Steiner[a], Ivan V. Kozhevnikov[a,*]

[a] *Department of Chemistry, University of Liverpool, Liverpool, L69 7ZD, United Kingdom*
[b] *Stephenson Institute for Renewable Energy, University of Liverpool, Liverpool, L69 7ZD, United Kingdom*
[c] *State Key Laboratory of Catalysis, Dalian Institute of Chemical Physics, Chinese Academy of Sciences, Dalian, 116023, China*

ARTICLE INFO

ABSTRACT

Keggin-type polyoxometalates (POM) immobilized on alkylaminophosphazene (RPN)-functionalized silica (POM/RPN-SiO$_2$) are new effective single-site solid catalysts for oxidative desulfurization (ODS) of diesel fuel under mild conditions in a biphasic system composed of a benzothiophene-containing model diesel fuel (heptane) and aqueous 30% H$_2$O$_2$. The catalytic activity of POM/RPN-SiO$_2$ was found to be influenced by the choice of POM and the amine R group in RPN, decreasing in the order PMo > PW > SiW and Bz > iBu > iPr, respectively. The most effective catalyst, PMo/BzPN-SiO$_2$ (PMo = PMo$_{12}$O$_{40}$$^{3-}$), exhibited 100% removal of dibenzothiophene from model diesel fuel at 60 °C and ambient pressure and could be reused without loss of activity. This catalyst outperforms other recently reported heterogeneous catalysts for ODS in similar systems. ^{13}C, ^{29}Si and ^{31}P MAS NMR, FTIR, SEM, BET and elemental analysis were used to characterize the structure of surface phosphazene and POM species in the new catalysts.

1. Introduction

Due to increasingly strict environmental regulations, the sulfur content of diesel fuels used in transportation vehicles has decreased dramatically from 2000 to 10 ppm over the last 20 years and further reduction in sulfur content is desired [1–3]. Hydrodesulfurization (HDS) is the most widely used technology for removing sulfur from diesel fuels, which is usually operated at high temperature (300–400 °C) and pressure (30–130 atm) using alumina-supported Co-Mo or Ni-Mo sulfided oxides as catalysts [2,3]. The main drawbacks of HDS are severe operating conditions and low desulfurization efficiency in the case of refractory benzothiophenes. Alternative desulfurization methods have been investigated in recent years including, among others, oxidative desulfurization (ODS) [4,5], extraction [6], adsorption [7] and bio-desulfurization [8]. ODS appears to be the most promising method for deep desulfurization of diesel fuel. Typically, it involves liquid-phase biphasic oxidation of organosulfur compounds with H$_2$O$_2$ at low temperatures (60–80 °C) and atmospheric pressure to yield sulfoxides and sulfones, which can be separated from the fuel by precipitation, extraction or adsorption [4,5]. This method is highly efficient for removing refractory aromatic sulfur compounds such as thiols and benzothiophenes, which are difficult to remove by HDS [3].

Many ODS catalysts have been reported. Polyoxometalates (POMs), in particular Keggin-type POMs, have demonstrated remarkable ODS activity [9–14]. These compounds comprise polyanions, XM$_{12}$O$_{40}$$^{m-}$, composed of oxygen-sharing MO$_6$ octahedra (typically M = Mo^{VI}, W^{VI} and V^V) encapsulating a central tetrahedron XO$_4$$^{n-}$ (X = P^V, Si^{IV}, *etc.*) [14]. In the presence of hydrogen peroxide, these POMs degrade to form active peroxopolyoxometalate species (peroxo-POM), *e.g.*, the Venturello peroxo complex, {PO$_4$[WO(O$_2$)$_2$]$_4$}$^{3-}$ [15]. Peroxo-POMs are highly active catalysts in various biphasic oxidations with hydrogen peroxide [16–19]. In these reactions, a phase transfer agent (PTA) is required to transfer the peroxo-POM species from the aqueous phase containing H$_2$O$_2$ to the substrate-containing organic or fuel phase. Most frequently, quaternary ammonium cations are used as the PTAs in such systems, including amino-modified high molecular weight alkene oligomers [19].

Cyclic and polymeric phosphazenes are renowned for their chemical and thermal robustness. They have been used as high-performance elastomers, fire retardants, polymeric electrolytes and in biomedical applications [20,21]. Previously, we have demonstrated that alkylaminocyclophosphazenes {(RNH)$_6$P$_3$N$_3$, labelled hereafter as RPN, R = benzyl, *iso*-butyl or *iso*-propyl} exhibit promising phase transfer properties in POM-catalyzed biphasic oxidations with H$_2$O$_2$, including

---

oxidative desulfurization [13,22]. The basic N-sites of the cyclophosphazene ring are protonated by heteropoly acids, H_nPOM, forming ion pairs, in which the POM anions are effectively encapsulated by extensive hydrogen bonding with the protonated RPNs [22]. The lipophilicity of the alkylamino groups in RPN renders the resulting POM-RPN aggregates soluble in the organic fuel phase. Moreover, the phase transfer efficiency of RPN can be tuned by varying the alkyl group, R [13,22].

A major drawback of homogeneous POM catalysts in PTA-assisted biphasic oxidative desulfurization is the difficulty of separating these catalysts from the fuel phase after desulfurization as the POM-PTA aggregates are highly soluble in the fuel phase. This would lead to contamination of fuel with POM. In this regard, heterogeneous ODS catalysts have the important advantage of easy catalyst separation from the fuel after reaction [23–27]. Here we report a new heterogeneous single-site catalyst POM/RPN-SiO₂ for the biphasic oxidative desulfurization of model diesel fuel by H_2O_2, which comprises Keggin POM chemically bound to silica surface via alkylaminocyclophosphazene tethers preventing the POM from leaching. This catalyst shows higher catalytic activity for the oxidation of benzothiophenes than its homogeneous analogue POM-RPN, with the advantage of easier catalyst separation and reuse. It is also superior in activity than other recently reported heterogeneous ODS catalysts in similar systems [25–27].

2. Experimental

2.1. Chemicals

Benzothiophene (BT, 99%), dibenzothiophene (DBT, 99%), 4,6-dimethyldibenzothiophene (DMBDT, 97%), heptane (99%), dodecane (99%), hexachlorocyclotriphosphazene, benzylamine, isobutylamine, isopropylamine, 30% H_2O_2, KMnO₄ (99%), H₂WO₄ (99%) and heteropoly acid hydrates $H_3PW_{12}O_{40}$ (99%), $H_3PMo_{12}O_{40}$ (99.9%) and H_4SiWO_{40} (99.9%) containing 20–28 H_2O molecules per Keggin unit were purchased from Sigma–Aldrich. Aminopropyl-functionalized silica Hypersil APS-2 (0.40 mmol g⁻¹ amino group loading (2.0 RNH₂ nm⁻²), 5 μm particle size) was purchased from Thermo Scientific. The amount of crystallization water in heteropoly acids was determined by thermogravimetric analysis (TGA).

2.2. Synthesis and characterization of RPN functionalized silica

Hypersil APS-2 (2.0 g, 0.80 mmol aminopropyl groups), dry toluene (40 mL), hexachlorocyclotriphosphazene $(P_3N_3Cl_6)$ (0.8 mmol) and triethylamine (20 mmol) were added to a 250 mL two-neck round bottomed flask equipped with a magnetic stirring bar, a reflux condenser and a bubbler. The flask was flushed with nitrogen at ambient temperature for 5 min (a dry atmosphere is required for the reaction, but not for the work-up). The mixture was then heated to reflux (120 °C) under nitrogen with stirring and left for 24 h. After the mixture was left to cool to room temperature, primary amine RNH₂ (R = benzyl (Bz), *iso*-butyl (iBu) or *iso*-propyl (iPr), 8.0 mmol) in dry toluene (10 mL) was added to the mixture. This was then heated to reflux (120 °C) with stirring for 24 h. The faint yellow/brown colored solution was then cooled to room temperature forming clear crystals (Et₃NH·HCl) and a yellow/brown powder. The mixture was filtered and washed with toluene under low pressure to produce a mixture of white powder/white crystals. These were transferred to a beaker with methanol (20 mL). The resulting creamy/white precipitate was stirred for 10 min and then filtered and washed with methanol to give a white powder. The powder was stirred with aqueous KOH (30 mL, 10% w/v) for 5 min to free any remaining amines from their chloride salts, filtered under low pressure, washed with distilled H_2O and dried under vacuum in a desiccator.

2.2.1. iBuPN-modified hypersil APS-2 (iBuPN-SiO₂)

Elemental analysis calcd (%) for 0.12 mmol g⁻¹ loading of iBuPN: C 3.13, N 1.55, P 1.16; found: C 3.69, N 1.87, P 1.15; FTIR (KBr powder, Hypersil APS-2 background): 3335 cm⁻¹ (ν_s N–H), 2963 cm⁻¹, 2876 cm⁻¹ (C–H$_{alkyl}$), 1466 cm⁻¹, 1406 cm⁻¹ (C–C$_{alkyl}$), 1114 cm⁻¹(ν_s P–N); δ ³¹P DE (Direct-Excitation with ¹H high power decoupling) NMR (161.9 MHz, 12 kHz MAS (Magic Angle Spinning)): (R'/R" = Pr or iBu), 18 and 14 ppm {P(NHR')NHR"}, 9 and 4 ppm {P(=O)NHR'}, −3 ppm (PO₂); δ ²⁹Si CP (Cross-Polarization) NMR (79.4 MHz, 10 kHz MAS): −59 ppm (T²), −67 ppm (T³), −102 ppm (Q³), −111 ppm (Q⁴); δ ¹³C CP NMR (100.5 MHz, 10 kHz MAS): 49, 30 and 19 ppm (iBuNH), 43, 25 and 10 ppm (PrNH); iBuPN loading was found to be 0.12 mmol g⁻¹ determined by P content from ICP analysis.

2.2.2. BzPN-modified hypersil APS-2 (BzPN-SiO₂)

Elemental analysis calcd (%) for 0.14 mmol g⁻¹ loading of BzPN: C 5.71, N 1.76, P 1.30; found: C 5.58, N 1.88, P 1.32. FTIR (KBr powder, Hypersil APS-2 background): 3403 cm⁻¹ (ν_{sym} N–H), 3248 cm⁻¹ (ν_s N–H broad), 3028 cm⁻¹ (C–H$_{arom}$), 2849 cm⁻¹ (C–H$_{alkyl}$), 1664 cm⁻¹, 1496 cm⁻¹ (C=C$_{arom}$), 1448 cm⁻¹ (C–C$_{alkyl}$), 1274 cm⁻¹, 1107 cm⁻¹ (ν_s P–N), 878 cm¹ (P–O), 731 cm⁻¹, 699 cm⁻¹ (C–H, arom); δ ³¹P DE NMR (161.9 MHz, 12 kHz MAS): (R'/R" = Pr or Bz), 19 and 14 ppm {P(NHR')NHR"}, 5 ppm {P(=O)NHR'}, −3 ppm (PO₂); δ ²⁹Si CP NMR (79.4 MHz, 10 kHz MAS): −59 ppm (T²), −67 ppm (T³), −102 ppm (Q³), −111 ppm (Q⁴); δ ¹³C CP NMR (100.5 MHz, 14 kHz MAS): 142, 128 and 45 ppm (BzNH), 43, 25 and 10 ppm (PrNH); BzPN loading was found to be 0.14 mmol g⁻¹ determined by P content from ICP analysis.
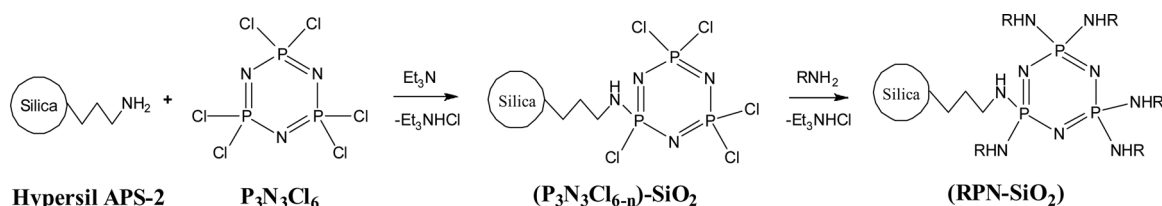
2.2.3. iPrPN-modified hypersil APS-2 (iPrPN-SiO₂)

Elemental analysis calcd (%) for 0.14 mmol g⁻¹ loading of iPrPN: C 3.02, N 1.76, P 1.30; found: C 3.17, N 1.73, P 1.29. FTIR (KBr powder, Hypersil APS-2 background): 3333 cm⁻¹ (ν_{sym} N-H), 3225 cm⁻¹ (ν_{sym} N-H broad), 2971 cm⁻¹, 2880 cm⁻¹ (C-H$_{alkyl}$), 1466 cm⁻¹, 1409 cm⁻¹ (C–C$_{alkyl}$), 1310 cm⁻¹ (ν_s P–N). 896 cm⁻¹ (P–O), 718 cm⁻¹, 650 cm⁻¹, 626 cm⁻¹; δ ³¹P DE NMR (161.9 MHz, 12 kHz MAS): (R'/R" = Pr or iPr), 18 and 12 ppm {P(NHR')NHR"}, 5 ppm {P(=O)R'}, −2 ppm (PO₂); δ ²⁹Si CP NMR (79.4 MHz, 10 kHz MAS): −59 ppm (T²), −67 ppm (T³), −102 ppm (Q³), −111 ppm (Q⁴); δ ¹³C CP NMR (100.5 MHz, 10 kHz MAS): 43 and 24 ppm (iPrNH), 43, 25 and 10 ppm (PrNH); iPrPN loading was found to be 0.14 mmol g⁻¹ determined by P content.

2.2.4. PMo/BzPN-SiO₂

$H_3PMo_{12}O_{40}$ (0.0332 g, 0.014 mmol), BzPN-SiO₂ (0.1 g, 0.014 mmol surface BzPN groups), H_2O (0.3 mL) and heptane (10 mL) was stirred in a 50 mL beaker at ambient temperature and pressure for 30 min. The product, a yellow powder, was then filtered under low pressure and washed with heptane. The powder was dried under vacuum overnight; it gradually turned yellow-green. Elemental analysis calcd (%) for [PMo]/[BzPN] = 1:1 mol/mol loading: C 4.55 and N 1.41; found: C 4.37, N 1.55. FTIR (KBr powder, Hypersil APS-2 background): 3577 cm⁻¹ (ν_{sym} N–H), 3346 cm⁻¹ (ν_{sym} N–H), 1408 cm⁻¹ (C–C$_{alkyl}$), 1328 cm⁻¹ (ν_s P–N), 1099 cm⁻¹ (P–O), 965 cm⁻¹ (Mo=O), 874 cm¹, 818 cm⁻¹ (Mo–O–Mo$_{bridge}$); δ ³¹P DE NMR (161.9 MHz, 12 kHz MAS): (R'/R" = Pr or Bz), 11 ppm {P(NHR')NHR"}, −3.7 and −4.4 ppm (PMo); δ ²⁹Si CP NMR (79.4 MHz, 10 kHz MAS): −59 ppm (T²), −67 ppm (T³), −102 ppm (Q³), −111 ppm (Q⁴); δ ¹³C CP NMR (100.5 MHz, 14 kHz MAS): 140, 128 and 45 ppm (BzNH), 43, 25 and 10 ppm (PrNH).

2.3. Reaction procedure for catalytic testing

Dodecane (GC internal standard, 0.40 mmol), DBT, BT or DMDBT (0.50 m mol), heptane (10 mL), POM (0.0056 mmol) and 30% H_2O_2 (0.15 mL, 1.51 mmol) were placed in a 50 mL jacketed glass reactor

Scheme 1. Grafting RPN onto aminopropyl-modified silica Hypersil APS-2.

vessel equipped with a magnetic stirrer, a heat circulator and a reflux condenser. The resulting mixture was stirred for 2 min at ambient temperature ($\sim 20\,^\circ$C) to activate the catalyst. RPN-SiO$_2$ (0.0056 mmol with respect to RPN) was added to start the reaction at the required temperature and stirring speed (60 $^\circ$C and 1500 rpm unless stated otherwise). Reaction rate did not depend on the stirring speed in the range of 1000–1500 rpm, which indicates no external diffusion limitation. The conversion of benzothiophenes was monitored by submitting aliquots of the organic phase for analysis by gas chromatography (GC) using the internal standard method (a Varian Chrompack CP-3380 gas chromatograph equipped with a flame ionization detector and a 25 m × 0.32 mm × 0.5 μm BP1 capillary column). The mean absolute percentage error in benzothiophene conversion was ≤10%.

For catalyst reuse, the initial reaction was run using the above procedure. After reaction had reached completion, the mixture was left to settle and the organic and aqueous layers were carefully decanted off. The catalyst powder in the reactor vessel was washed with 2 × 5 mL of acetonitrile to remove the sulfone product then washed with heptane (5 mL) using a centrifuge. The catalyst was dried at ambient temperature overnight. The dried catalyst was added back to the reactor along with 30% H$_2$O$_2$ (0.15 mL, 1.51 mmol), dodecane (0.40 mmol), benzothiophene (0.50 mmol) and heptane (10 mL) for the next run.

2.4. Techniques

BET analysis of catalyst samples was conducted on a Micrometrics ASAP 2010 instrument by N$_2$ physisorption at −196 $^\circ$C. Samples were pre-treated at 140 $^\circ$C under vacuum for 4.5 h. Fourier transform infrared (FTIR) spectra were recorded in DRIFTS (diffuse reflectance infrared Fourier transform spectroscopy) mode on a Nicolet Nexus FTIR spectrometer using powdered catalyst mixtures with KBr. Phosphorus content in catalysts was determined on a Spectro Ciros ICP-OES analyzer, with samples prepared by digesting 0.02 g of a catalyst sample in 1:3 aqua regia (4 mL), which was then made up to 10 mL with distilled H$_2$O.

All NMR experiments were performed on a 400 DSX NMR spectrometer, using a 4 mm HXY probe in triple resonance mode with the X channel tuned to ^{31}P at 161.9 MHz, and Y channel tuned to ^{13}C at 100.5 MHz in ^{13}C CP experiments and to ^{29}Si at 79.4 MHz in ^{29}Si CP experiments, respectively.

2.4.1. P DE NMR

Experiments were performed at a magic angle spinning (MAS) rate of 12 kHz using ^{31}P rf (radio-frequency) field amplitude pulses and ^{1}H cw (continuous-wave) decoupling at 83 kHz. 128–2048 transients were accumulated with a quantitative recovery delay longer than 5 x T$_1$. The

chemical shifts were referenced to aqueous 85% H$_3$PO$_4$ at 0 ppm.

2.4.2. C CP NMR

Experiments were performed at MAS rates of 10 and 14 kHz. The rf field amplitude of ^{1}H 90° pulses and SPINAL64 decoupling were 83 kHz [28]. For ^{1}H to ^{13}C CP transfer, the amplitude-ramped rf field for ^{1}H was 60 kHz, while Hartmann-Hahn matched ^{13}C rf field was 25–33 kHz at MAS rate of 10 kHz and 30–53 kHz at MAS rate of 14 kHz, and the contact time was optimized to be 1–2 ms. 5120 to 47104 transients were accumulated with a recovery delay of 3 s per transient. The chemical shifts were referenced to CH of adamantane at 29.45 ppm [29].

2.4.3. Si CP NMR

Experiments were performed at a MAS rate of 10 kHz. The rf field amplitude of ^{1}H 90° pulse and SPINAL64 decoupling was 83 kHz [28]. For ^{1}H to ^{29}Si CP transfer, the amplitude-ramped rf field for ^{1}H was 60 kHz, while Hartmann-Hahn matched ^{29}Si rf field was 28–57 kHz, and the contact time was optimized to be 9 ms. 20480–51200 transients were accumulated with a recovery delay of 3 s per transient. The chemical shifts were referenced to the most upfield signal of Q$_8$M$_8$ at −109 ppm (corresponding to SiMe$_4$ at 0 ppm) [30].

Scanning electron microscopy (SEM) was performed on an FEI Quanta 250 FEG Environmental SEM, operating in "low vacuum" mode. This allowed for imaging of non-conductive samples by filling the sample chamber with a small amount of pure water vapor (at 100 Pa), which helped dissipate beam induced charge from the sample surface. To image the samples, the dry powder silica particles were deposited directly on double-sided carbon adhesive discs (*Agar Scientific*). All images were obtained at low beam energy (5 kV) to avoid sample damage and charging effects.

3. Results and discussion

3.1. Phosphazene-modified silica support

The route for grafting alkylaminocyclotriphosphazenes onto silica is shown in Scheme 1. First, the reaction of hexachlorocyclotriphosphazene (P$_3$N$_3$Cl$_6$) with Hypersil APS-2 in the presence of triethylamine produced the chlorocyclotriphosphazene grafted silica (P$_3$N$_3$Cl$_{6-n}$)-SiO$_2$ (where n is the number of grafted aminopropyl linkers; in Scheme 1, n = 1 as an example). Subsequent reaction with an 8-fold molar excess of RNH$_2$ yielded the final RPN functionalized silica, RPN-SiO$_2$.

Elemental analysis of the prepared RPN-SiO$_2$ samples is given in Table 1. It provided empirical formulae C$_{32.4}$N$_{9.4}$P$_3$, C$_{24.8}$N$_{10.8}$P$_3$ and C$_{18.9}$N$_{8.9}$P$_3$ for BzPN-SiO$_2$, iBuPN-SiO$_2$ and iPrPN-SiO$_2$, respectively. This confirms the immobilization of the cyclophosphazenes on the silica

Table 1
Composition of RPN-SiO$_2$ samples.

RPN-SiO$_2$	Total N mmol g^{-1}	C mmol g^{-1}	P mmol g^{-1}	Ring N mmol g^{-1}	Amine N mmol g^{-1}	RPN mmol g^{-1}	C/Amine N
Hypersil APS-2	0.40	1.20	–	–	–	–	–
iPrPN-SiO$_2$	1.24	2.64	0.42	0.42	0.82	0.14	3.2
iBuPN-SiO$_2$	1.11	2.61	0.37	0.37	0.74	0.12	3.5
BzPN-SiO$_2$	1.34	4.65	0.43	0.43	0.92	0.14	5.0

surface and substitution of the cyclotriphosphazene chlorine with the RNH_2 alkylamines. The sources of nitrogen atoms in these samples are the N atoms of cyclotriphosphazene rings (three N atoms per ring, N:P = 1:1), as well as the Hypersil APS-2 aminopropyl groups and the RPN substituent amino groups RNH, each possessing a single nitrogen atom. As there are equimolar quantities of P and N present in cyclotriphosphazene rings, the P content was used to determine the quantity of nitrogen provided by the ring nitrogen atoms and the RPN loading for each RPN-SiO$_2$. The loading of the RPN on the silica surface thus calculated was $0.12\ mmol\ g^{-1}$ for iBuPN and $0.14\ mmol\ g^{-1}$ for iPrPN and BzPN. The total concentration of aminopropyl linker plus alkylamino substituent (Amine N) equals the difference between the total N and the total P content. The ratio of C/Amine N content for each RPN-SiO$_2$ approximates the distribution of the primary amino groups (RNH) and aminopropyl linkers in each sample (*e.g.*, for BzNH$_2$ and aminopropyl, the C/N ratio is 7 and 3, respectively, and equimolar amounts of both groups in BzPN-SiO$_2$ would give a [C]/[Amine N] ratio of 5, such as the value that was calculated using the experimental data).

Further, solid-state ^{13}C, ^{29}Si and ^{31}P MAS NMR, FTIR and elemental analysis were used to characterize the structure of surface phosphazene species formed in more detail, as well as to monitor the synthesis of RPN-SiO$_2$. The NMR data (Fig. S1–S4) indicated partial hydrolysis of PCl$_2$ groups in the initial stage of RPN grafting (Scheme 1) and the presence of phosphazene P=O and P−OH groups in the RPN-SiO$_2$ prepared. This is evidenced by the similarity of ^{31}P NMR shifts of the RPN-SiO$_2$ samples with hydrolyzed RPN species in solution reported previously [31], which is also supported by elemental analysis. These results are presented and discussed in detail in the Supporting Information. Taking the partial hydrolysis into account, more realistic structures of RPN grafted on Hypersil APS-2 can be represented as shown in Scheme 2 (cf. the idealized structure of RPN-SiO$_2$ shown in Scheme 1).

Fig. 1 shows the SEM images of Hypersil APS-2 and BzPN-functionalized Hypersil APS-2 (BzPN-SiO$_2$). The initial Hypersil APS-2 sample exhibits a uniform array of spherical particles of ~5 μm particle size. It can be seen that this morphology is preserved in the BzPN-functionalized sample, indicating that RPN grafting does not affect the morphology of the initial silica support.

The surface area and porosity of Hypersil ASP-2 and the functionalized supports RPN-SiO$_2$ are given in Table 2, together with the loading of surface functional groups determined by elemental analysis. These data show that RPN functionalization had a relatively small effect on the BET surface area due to small RPN loadings, although it slightly reduced the pore volume and pore diameter of the samples. Apparently, the RPN groups on the inside of pore walls of RPN-SiO$_2$ take up more space inside the pores than the aminopropyl groups of Hypersil APS-2, resulting in a decrease in the diameter and volume of pores of RPN-SiO$_2$
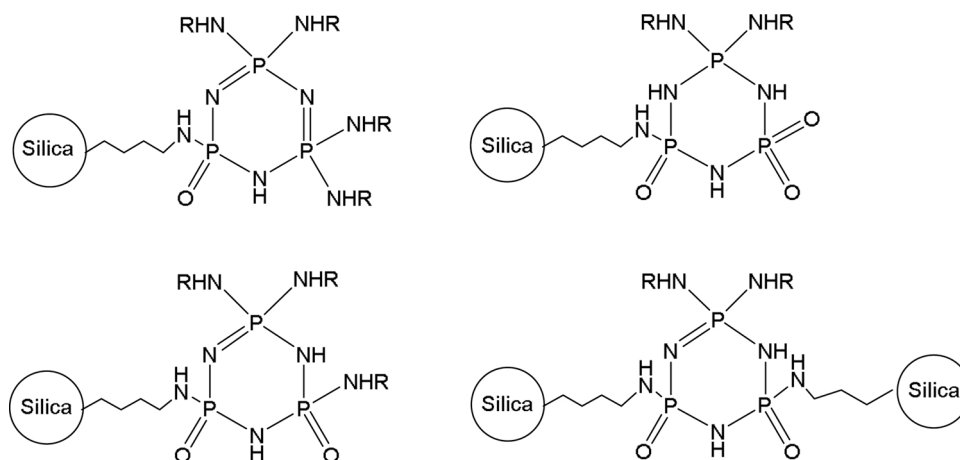
compared to Hypersil APS-2. The N$_2$ adsorption isotherms for Hypersil ASP-2 and BzPN-SiO$_2$ show a type IV isotherm with a H1 hysteresis loop (Fig. 2). This indicates a mesoporous structure of uniformly arranged spherical particles [32,33], in agreement with the SEM data (Fig. 1). The adsorption isotherms for iPrPN-SiO$_2$ and iBuPN-SiO$_2$ samples (Fig. S5) also show type IV isotherms with H1 hysteresis loops, which indicates that the mesoporous structure of the silica support remained intact through the RPN functionalization process.

3.2. POM immobilized on phosphazene-functionalized silica

Next, Keggin POMs, namely $PW_{12}O_{40}^{3-}$ (PW), $PMo_{12}O_{40}^{3-}$ (PMo) and $SiW_{12}O_{40}^{4-}$ (SiW), were immobilized onto the RPN-functionalized silica supports using the corresponding heteropoly acids as POM precursors (Sect. 2.2). This allowed us to obtain single-site catalysts comprising POM active species chemically bound (tethered) to the silica surface and spatially separated from each other. These catalysts were then used for the oxidative desulfurization of model fuel with H$_2$O$_2$. Among the POM/RPN-SO$_2$ catalysts, PMo/BzPN-SiO$_2$ (PMo/ BzPN = 1:1 mol/mol) showed the best desulfurization performance (see below); this catalyst was characterized in more detail by SEM, BET, solid-state NMR and FTIR.

Fig. 3 shows the SEM images of fresh and spent PMo/BzPN-SiO$_2$ catalysts, the latter was recovered after ODS of DBT (see below). Both catalysts have similar morphologies to those of Hypersil APS-2 and BzPN-SiO$_2$ (Fig. 1), which indicates that the loading of PMo and desulfurization reaction have little effect on catalyst morphology as confirmed by the surface and porosity data for fresh PMo/BzPN-SiO$_2$ catalyst (Table 2). It should be noted, however, that fresh PMo/BzPN-SiO$_2$ had a higher quantity of smaller particles attached onto the surface as compared to the spent catalyst (Fig. 3). Possibly, the smaller particles were washed out during the ODS reaction. PMo/BzPN-SiO$_2$ also displayed a type IV nitrogen adsorption isotherm with a H1 hysteresis loop (Fig. S5), similar to those for Hypersil ASP-2 and BzPN-SiO$_2$ (Fig. 2), which corroborates with the SEM images above suggesting that the catalyst particles remained spherical and fairly uniform after PMo loading.

The ^{13}C CP MAS NMR spectrum of PMo/BzPN-SiO$_2$ (Fig. 4A) shows the typical signals from the benzylamino groups (cf. the ^{13}C spectrum of BzPN-SiO$_2$ in Fig. S2), while the ^{29}Si CP MAS NMR spectrum (Fig. 4B) confirms the presence of T^2 and T^3 signals (cf. Fig. S3), suggesting that the structure of BzPN-SiO$_2$ remained intact after loading PMo. In the ^{31}P MAS NMR spectrum (Fig. 4C), two sharp peaks at −3.7 and −4.4 ppm can be assigned to PMo and its hydrate [34,35] confirming the presence of intact PMo in the catalyst. The broad peak of BzPN in PMo/BzPN-SiO$_2$ is shifted upfield from 14 ppm to 11 ppm as compared to BzPN-SiO$_2$ (Fig. S2), which suggests protonation of one or two of the

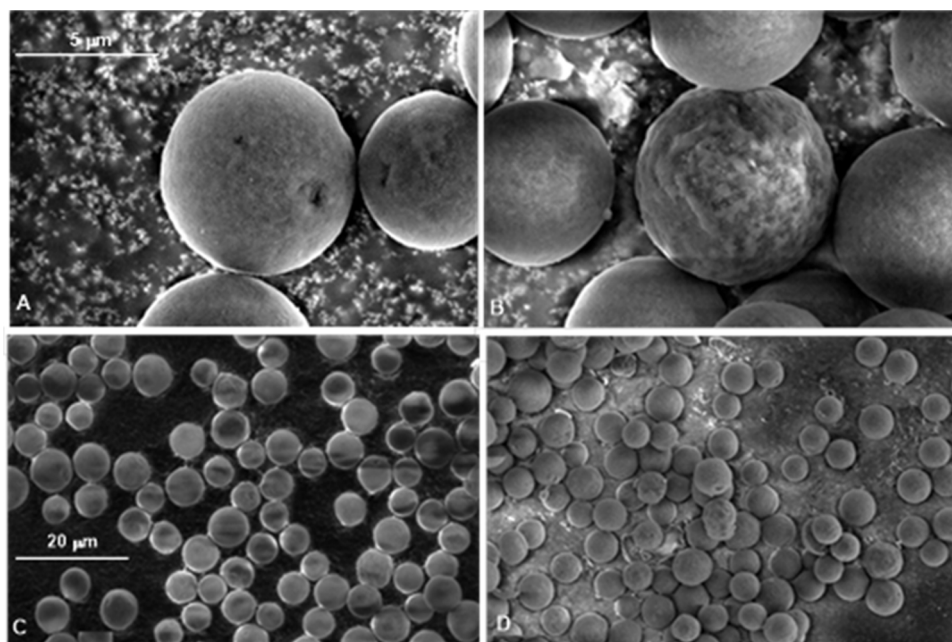**Scheme 2.** Probable surface structures of RPN-modified Hypersil APS-2.

Fig. 1. SEM images of Hypersil APS-2 (A, C) and BzPN-SiO$_2$ (B, D); magnification scale 5 μm for A, B and 20 μm for C, D.

Table 2
Surface and porosity data for Hypersil APS-2 and RPN-SiO$_2$ functionalized supports.[a]

Sample	RPN loading mmol g^{-1}	S_{BET}[b] m^2 g^{-1}	Pore volume[c] cm^3 g^{-1}	Pore diameter[d] Å
Hypersil APS-2	0.40[e]	123	0.54	174
iPrPN-SiO$_2$	0.14	130	0.49	151
iBuPN-SiO$_2$	0.12	109	0.39	144
BzPN-SiO$_2$	0.14	116	0.42	143
PMo/BzPN-SiO$_2$	0.14	122	0.41	135

[a] Samples pre-treated at 140 °C under vacuum.
[b] BET surface area.
[c] Single point total pore volume.
[d] Average pore diameter.
[e] Loading of aminopropyl groups.

phosphazene nitrogens [13].

The PMo/BzPN-SiO$_2$ catalyst exhibited characteristic peaks of the Keggin anion PMo$_{12}$O$_{40}$$^{3-}$ in the FTIR spectrum (Fig. 5) at 962 cm^{-1} (Mo=O), 873 cm^1 (Mo−O−Mo corner-sharing) and 794 cm^{-1} (Mo−O−Mo edge-sharing) [36], which indicates that PMo remained intact in the catalyst. The intense peak at 1065 cm^{-1} (P−O) in the FTIR spectrum of PMo/BzPN-SiO$_2$ is obscured by the broad silica band at

1000–1300 cm^{-1}.

Previously, single-crystal X-ray diffraction has been used to characterize the bonding in bulk POM-RPN aggregates [22]. It has been found that the POM structures remain intact upon aggregation with RPNs, where the Keggin units are encapsulated by RPNH$^+$ and RPNH$_2$$^{2+}$ cations through ionic and hydrogen bonding. As ^{31}P MAS NMR (Fig. 4C) and FTIR (Fig. 5) indicate that the structure of PMo in PMo/BzPN-SiO$_2$ is intact, we can suggest that POM is grafted onto the silica support through ionic and hydrogen bonding with cationic BzPNH$^+$ and BzPNH$_2$$^{2+}$ species. These cationic species are formed by protonation of BzPN with H$_3$PMo$_{12}$O$_{40}$ during the preparation procedure.

3.3. Oxidation of benzothiophenes by H$_2$O$_2$ catalyzed by POM/RPN-SiO$_2$

Here the prepared POM/RPN-SiO$_2$ catalysts comprising Keggin-type polyoxometalates (PMo, PW and SiW) immobilized onto the RPN-functionalized silica support were used for oxidative desulfurization of model diesel fuel by H$_2$O$_2$ in a biphasic heptane-H$_2$O system, with heptane as a model fuel and benzothiophene (BT, DBT or DMDBT) as an organosulfur compound. Most of the work was carried out with DBT because the oxidation of DBT is typically employed as a model reaction for testing desulfurization catalysts, hence it is easy to compare results with those obtained in different catalyst systems. The desulfurization
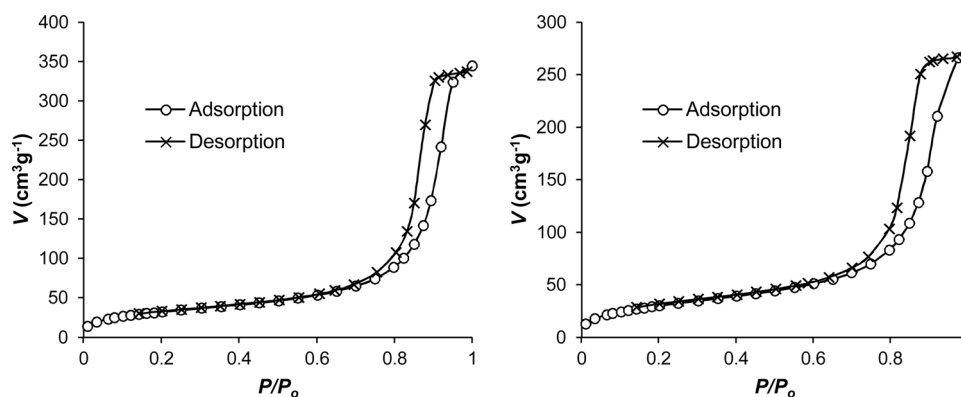

Fig. 2. Nitrogen adsorption isotherm for Hypersil APS-2 (left) and BzPN-SiO$_2$ (right).
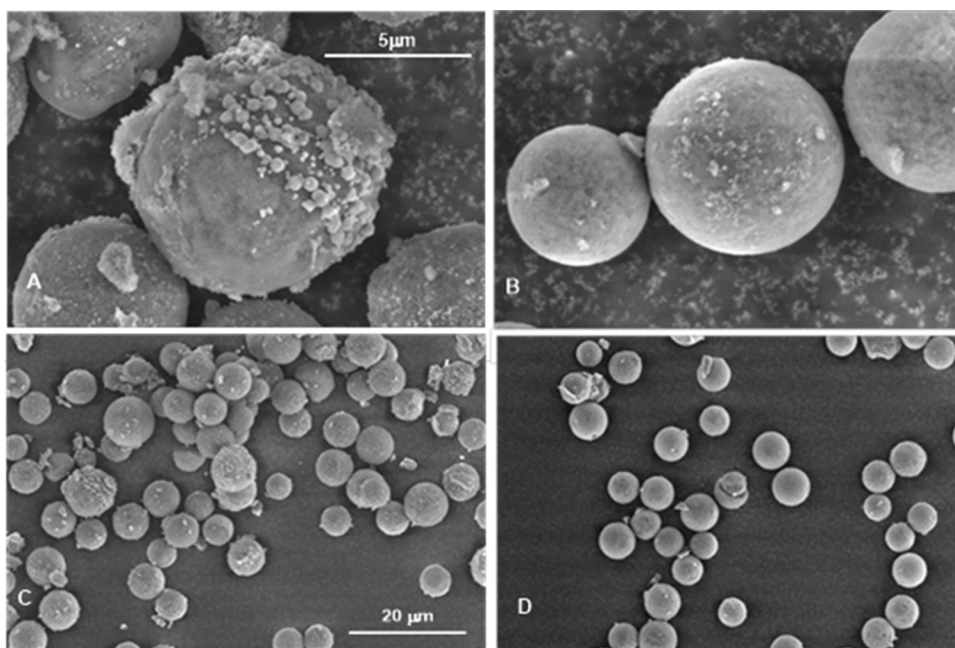
Fig. 3. SEM images of fresh PMo/BzPN-SiO$_2$ catalyst (A, C) and spent catalysts (B, D) recovered after desulfurization reaction; magnification scale 5 μm for A, B and 20 μm for C, D.

process involved oxidation of benzothiophenes to the corresponding sulfones as shown in Scheme 3 for the oxidation of DBT. In these experiments, the POM/RPN-SiO$_2$ catalysts were assembled in situ by adding POM (as the corresponding heteropoly acid) and RPN-SiO$_2$ separately to the reaction mixture to ensure more efficient activation of the POM by hydrogen peroxide prior to reaction (Sect. 2.3).

Representative results are given in Table 3. The catalytic activity of POMs in the oxidation of DBT was found to decrease of the order PMo > PW > SiW (entries 3–5 in Table 3, Fig. 6) in agreement with both the relative stability of these POMs to degradation in aqueous solution and their oxidation potentials [14,37]. Of these POMs, PMo is the strongest oxidant and least stable toward degradation with H$_2$O$_2$, leading to more efficient formation of the active peroxo-POM species [14,37]. The same activity trend has been found previously in biphasic systems with homogeneous POM catalysts [13]. The reaction with XM/BzPN-SiO$_2$ (X = P, Si; M = Mo, W) can be represented by equations
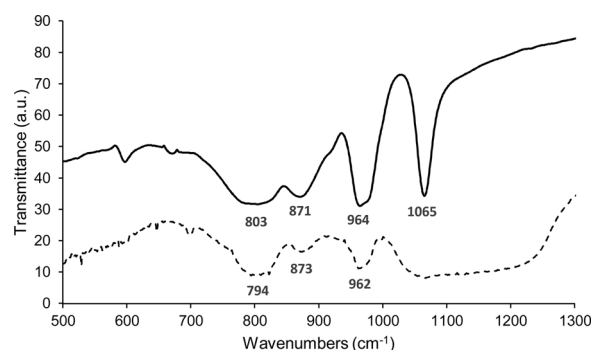

Fig. 5. FTIR spectra of PMo/BzPN-SiO$_2$ (dashed line) and H$_3$PMo$_{12}$O$_{40}$ (solid line) (KBr powder).
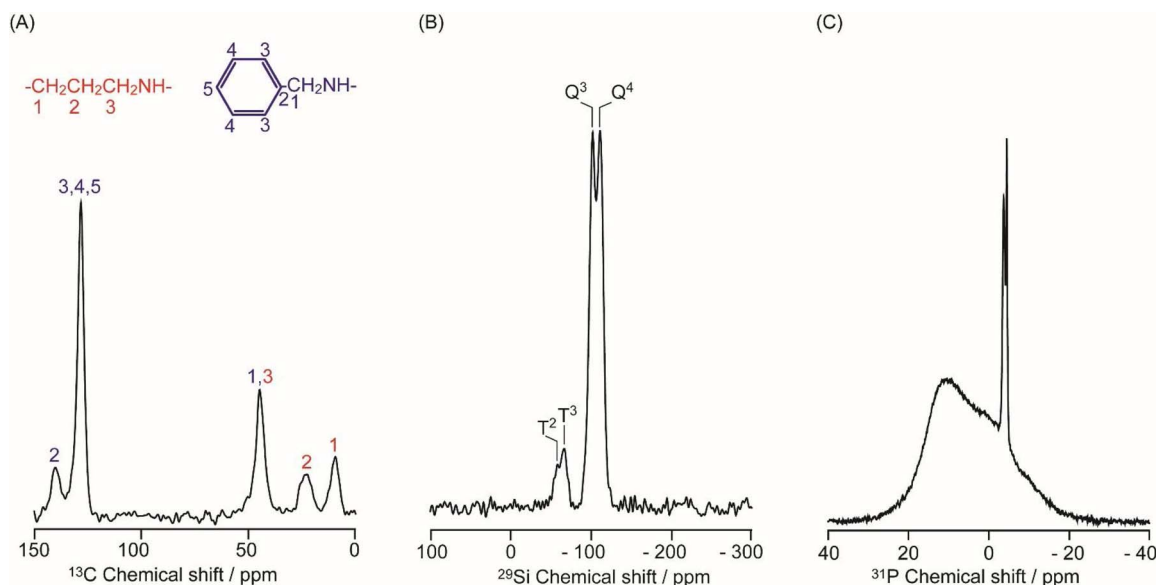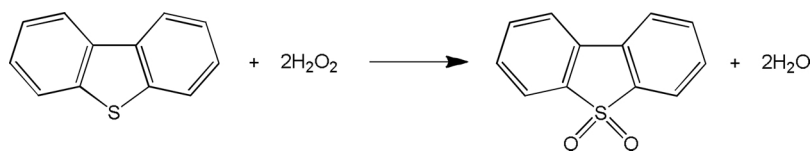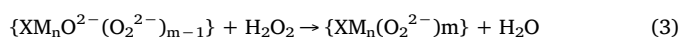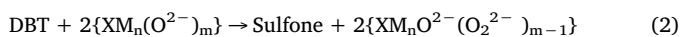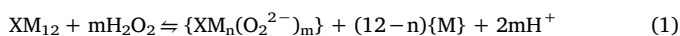

Fig. 4. (A) ^{13}C CP MAS (14 kHz), (B) ^{29}Si CP MAS (10 kHz) and (C) ^{31}P DE MAS (12 kHz) NMR spectra for PMo/BzPN-SiO$_2$.

Scheme 3. Oxidation of DBT to sulfone by H_2O_2.

(1)–(3) as with homogeneous XM-RPN catalysts [13]. The Keggin POM precursor initially degrades in the presence of H_2O_2 to form the active peroxo species (step 1), which oxidizes DBT to sulfone (step 2) and finally regenerates to reform the active peroxo species (step 3). Steps (1) and (3) occur in the aqueous phase or at the interface, and step (2) in the organic phase. With the least stable POM, PMo, step (1) is likely to occur faster than with PW and SiW, which can explain the relative catalyst activity of these POMs.

$$XM_{12} + mH_2O_2 \leftrightarrows \{XM_n(O_2^{2-})_m\} + (12-n)\{M\} + 2mH^+ \tag{1}$$

$$DBT + 2\{XM_n(O^{2-})_m\} \rightarrow Sulfone + 2\{XM_nO^{2-}(O_2^{2-})_{m-1}\} \tag{2}$$

$$\{XM_nO^{2-}(O_2^{2-})_{m-1}\} + H_2O_2 \rightarrow \{XM_n(O_2^{2-})m\} + H_2O \tag{3}$$

Entries 1 and 2 in Table 3 compare the catalytic activity of PMo/Hypersil APS-2 and PMo/BzPN-SiO$_2$ single-site catalysts, which had the same PMo loading, with molecular dispersion of PMo Keggin units. As can be seen, PMo/BzPN-SiO$_2$ is a significantly more efficient catalyst for the oxidation of DBT than PMo/Hypersil APS-2 (96 and 32% DBT conversion at 60 °C in 2 h, respectively). The corresponding initial turnover frequencies for these catalysts were calculated to be 1.9 and 0.24 min^{-1}, *i.e.*, PMo/BzPN-SiO$_2$ is 8 times more active than PMo/Hypersil APS-2 in terms of turnover rates. This shows that RPN groups in the POM/RPN-SiO$_2$ catalysts are better tethers for catalytically active POM species on silica than aminopropyl groups of the parent Hypersil APS-2. This can be attributed to the RPN groups that enhance the hydrophobic character of RPN-SiO$_2$ compared to Hypersil APS-2. With respect to the RPN groups, the catalytic activity decreases in the order BzPN > iBuPN > iPrPN (Table 3, entries 3, 6 and 7; Fig. S6), in line with decreasing the size of the R group. The best performance of the BzPN group may be attributed to arene-arene π-π interactions between the BzPN benzene ring and benzothiophene molecules, which may enhance the catalytic activity by increasing the local concentration of benzothiophene around the active sites. Another contributing factor may be the basicity of the phosphazene ring, which is affected by the primary amine substituent groups [38]. Increased basicity would strengthen the interaction between precursor heteropoly acid and the RPN surface group.

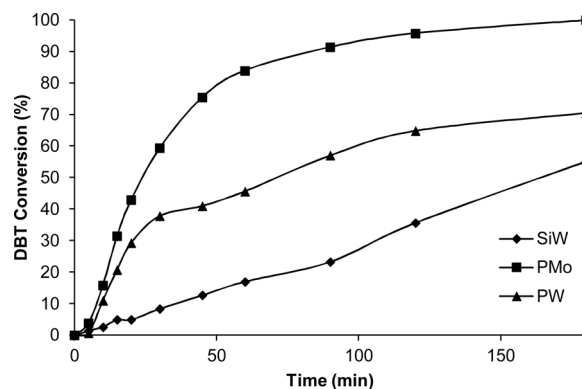The reactivity of benzothiophenes was found to decrease in the

Fig. 6. Comparison of activity of POM/BzPN-SiO$_2$ catalysts (POM/BzPN = 1:1 mol/mol) in DBT oxidation by H_2O_2 in heptane-H_2O two-phase system (60 °C, POM (0.0056 mmol), 30% H_2O_2 (0.15 mL, 1.51 m mol), DBT (0.50 m mol), heptane (10 mL)).

order DBT > DMDBT > BT (Table 3, entries 3, 10 and 12). The same trend has also been observed in homogeneous systems [4,5,9,10,13,39,40]. It can be attributed to the electron density on the S atom and steric effects of the methyl groups in DMDBT [10]. The electron density on the S atom increases in the order BT < DBT ≈ DMDBT, which can explain the lower reactivity of BT as compared to DBT and DMDBT. On the other hand, the S atom in DMDBT is sterically hindered by the two neighboring methyl groups rendering it less reactive compared to DBT [10].

As expected, the reaction rate increased with increasing the temperature (Fig. S7). For the oxidation of DBT with PMo/BzPN-SiO$_2$ catalyst, the apparent activation energy was found to be 47 kJ mol^{-1} in the temperature range 40–60 °C (see the Arrhenius plot in Fig. S8). This value is high enough to indicate the absence of significant diffusion limitations in the reaction system.

Notably, the PMo/BzPN-SiO$_2$ catalyst was found to be more active than its homogeneous analogue PMo-BzPN, which has been reported previously [13]. PMo/BzPN-SiO$_2$ (PMo/BzPN = 1:1) gave 94% DBT conversion in 2 h at 50 °C, whereas PMo/BzPN gave only 28 and 49% with an 1:1 and 1:6 PMo/BzPN molar ratio, respectively, under the same reaction conditions and at the same PMo loading (Fig. 7) [13].

Table 3
Oxidation of benzothiophenes by H_2O_2 in heptane-H_2O system using POM/RPN-SiO$_2$ as catalysts.[a]

Entry	POM/RPN mol/mol	POM	RPN	Benzothiophene	Temp. °C	Time h	Conv.%	H_2O_2 efficiency[c] %
1	1:4	PMo	PrNH$_2$[b]	DBT	60	2	32	22
2	1:1	PMo	BzPN	DBT	60	2	96	68
3	1:1	PMo	BzPN	DBT	60	3	100	68
4	1:1	PW	BzPN	DBT	60	3	70	50
5	1:1	SiW	BzPN	DBT	60	3	55	52
6	1:1	PMo	iBuPN	DBT	60	3	86	61
7	1:1	PMo	iPrPN	DBT	60	3	61	55
8	1:1	PMo	BzPN	DBT	50	3	100	68
9	1:1	PMo	BzPN	DBT	40	3	81	69
10	1:1	PMo	BzPN	BT	60	3	57	
11	1:1	PMo	BzPN	BT	60	6	90	80
12	1:1	PMo	BzPN	DMDBT	60	3	86	
13	1:1	PMo	BzPN	DMDBT	60	4	100	65

[a] POM (0.0056 mmol), 30% H_2O_2 (0.15 mL, 1.51 mmol), dodecane (GC standard, 0.40 mmol), benzothiophene (0.50 mmol) and heptane (10 mL); molar ratio [benzothiophene]/[H_2O_2] = 1:3, [POM]/[H_2O_2] = 1:270 and [POM]/[benzothiophene] = 1:90; stirring speed 1500 rpm.
[b] Unmodified Hypersil APS-2.
[c] Reaction selectivity with respect to H_2O_2 determined from titration of unconverted H_2O_2 with KMnO$_4$.
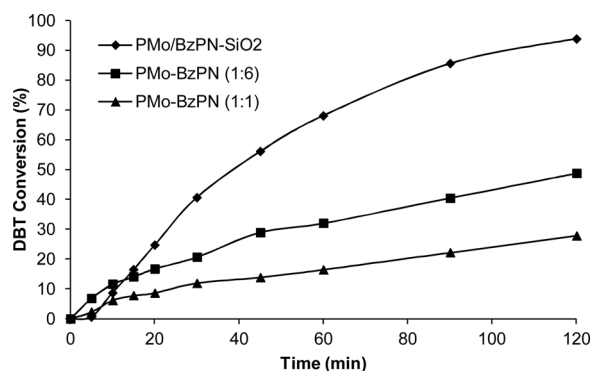
Fig. 7. Comparison of heterogeneous PMo/BzPN-SiO$_2$ (PMo/BzPN = 1:1) and homogeneous PMo-BzPN (PMo/BzPN = 1:1 or 1:6) catalysts for oxidation of DBT with H$_2$O$_2$ (50 °C, PMo (0.0056 mmol), 30% H$_2$O$_2$ (0.15 mL, 1.51 mmol), DBT (0.50 mmol) and heptane (10 mL)).

Table 4
Comparison of heterogeneous catalysts for oxidation of DBT in model diesel fuel with H$_2$O$_2$.[a]

Catalyst	Model diesel	DBT/ H$_2$O$_2$ mol/mol	T °C	Time h	DBT conversion %	Reference
PMo/BzPN-SiO$_2$	heptane	1:3	60	3	100	This work
Ti(IV)/SiO$_2$	isooctane	1:5	60	8	99	[25]
Zr(IV)/ PMMA-[b]	n-octane	1:3.5	65	24	84	[26]
PW$_{11}$Zn-MOF[c]	n-octane	1:50	50	6	100	[27]

[a] Biphasic systems comprising a model diesel phase and aqueous H$_2$O$_2$ phase.
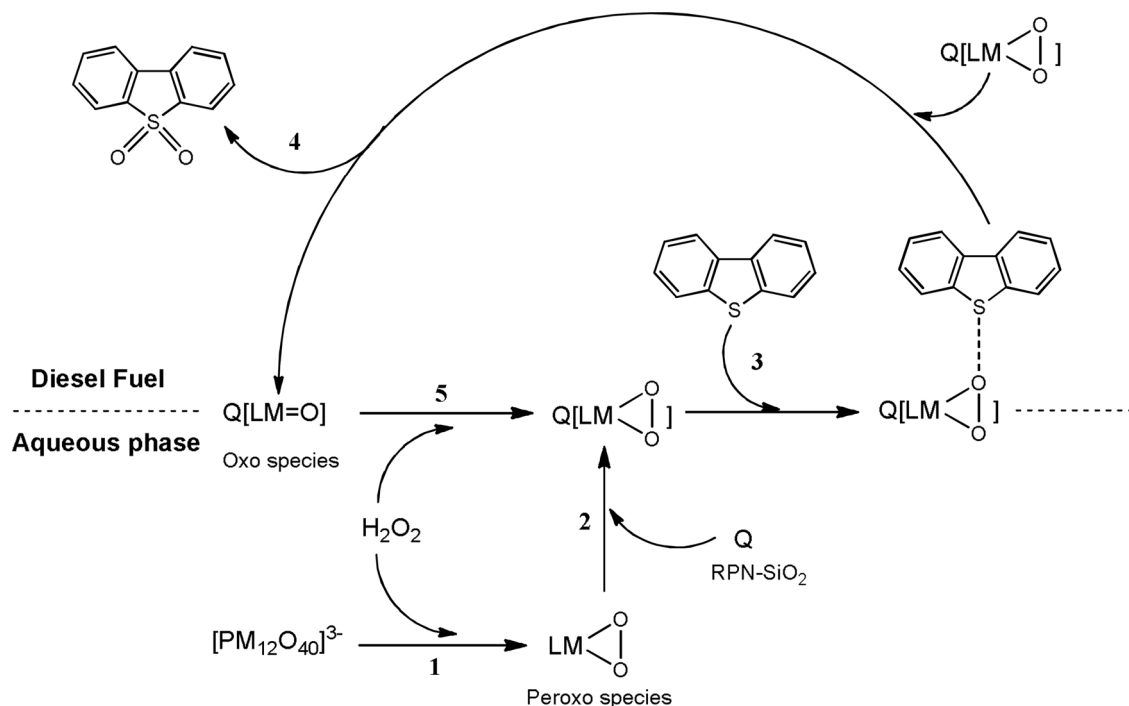[b] Zr(IV) oxoclusters in poly(methylmethacrylate) matrix (PMMA).
[c] MOF comprising PW$_{11}$Zn polyoxometalate and 2-aminoterephthalic acid in n-octane – [BIMIM]PF$_6$ biphasic system.

This may be explained by adsorption of DBT onto the surface of PMo/BzPN-SiO$_2$ silica support, which could increase the local concentration of DBT around the active catalyst sites. In addition, interaction between the active surface groups and DBT may be aided by the flexible aminopropyl tethers between silica and BzPN, which increase the mobility of the active peroxo-POM/BzPN units at the silica surface.

The PMo/BzPN-SiO$_2$ catalyst has an important advantage over its homogeneous analogue of easy and clean catalyst separation from fuel by simple filtration. The solid PMo/BzPN-SiO$_2$ catalyst could be easily recovered and, after washing with acetonitrile or toluene to remove the sulfone product, reused at least three times in the oxidation of DBT at 60 °C, giving 100% DBT conversion after each use.

The PMo/BzPN-SiO$_2$ catalyst showed higher activity than other heterogeneous catalysts that have been reported recently for the oxidation of DBT with hydrogen peroxide in similar systems [25–27] (Table 4). For example, Ti(IV) grafted onto silica gives 99% DBT conversion to sulfone in isooctane with 10–60% H$_2$O$_2$ at 60 °C in 8 h reaction time [25]. With hybrid catalysts comprising Zr(IV) and Hf(IV) oxoclusters in poly(methylmethacrylate) matrix, 84% DBT conversion to sulfone with 94% selectivity has been obtained in n-octane with 30% H$_2$O$_2$ at 65 °C in 24 h [26]. A polyoxometalate-MOF composite comprising PW$_{11}$Zn and 2-aminoterephthalic acid in n-octane–[BIMIM]PF$_6$ biphasic system at 50 °C gives 70% DBT conversion in 4 h and ~100% in 6 h reaction time, however this was obtained using a 50-fold molar excess of 30% H$_2$O$_2$ over DBT [27]. In this system, the ionic liquid [BIMIM]PF$_6$ has been used to extract the product sulfone from the model diesel. In comparison with these catalysts, our PMo/BzPN-SiO$_2$ catalyst gave 100% DBT conversion in heptane with 30% H$_2$O$_2$ at DBT/ H$_2$O$_2$ = 1:3 mol/mol and 60 °C in 3 h reaction time to deliver the best result.

The proposed reaction scheme for oxidation of DBT in model diesel fuel by H$_2$O$_2$ catalyzed by POM/RPN-SiO$_2$ is shown in Scheme 4. In the initial step, POM degrades in the presence of H$_2$O$_2$ in the aqueous phase to form a catalytically active peroxopolyoxometalate species (1) [14]. This species is then heterogenized by interaction with the surface RPN groups of the RPN-SiO$_2$ support (2) via ionic and hydrogen bonding. Next, the supported peroxopolyoxometalate species oxidize DBT to DBT sulfone (3). The sulfone, poorly soluble in heptane and insoluble in

Scheme 4. Reaction scheme for oxidation of DBT by H$_2$O$_2$ catalyzed by POM/RPN-SiO$_2$ in two-phase system.

water, precipitates out (4). The supported POM, now reduced to an oxo species, is regenerated by H_2O_2 from the aqueous phase to reform the active peroxo-POM species (5), thus completing the catalytic cycle. In this multiphase system, intense stirring is essential to facilitate the heterogeneously catalyzed oxidation process. Sulfur-free diesel fuel can be separated from the catalyst and sulfone product by filtration once the reaction is complete. The sulfone can be separated from the catalyst by solvent extraction (with acetonitrile or toluene), and the catalyst can be reused.

4. Conclusions

In this work, phosphazene-modified silica supports, RPN-SiO₂ (R = benzyl, *iso*-butyl or *iso*-propyl) were prepared by grafting phosphazenes (RPN) onto commercially available Hypersil APS-2 aminopropyl-modified silica. Keggin-type polyoxometalates (PMo, PW and SiW) were immobilized onto the RPN-SiO₂ supports using the corresponding heteropoly acids as precursors to afford single-site POM/RPN-SiO₂ catalysts. The prepared POM catalysts were tested in a biphasic heptane-H₂O system for oxidative desulfurization (ODS) of a model diesel fuel (heptane containing benzothiophenes) with hydrogen peroxide as the oxidant. It was demonstrated that the most effective catalyst, PMo/BzPN-SiO₂, has a higher ODS activity than its previously reported homogeneous analogue, PMo-BzPN, with the advantage of easier catalyst separation and reuse due to the inherent heterogeneity provided by the phosphazene-functionalized silica support. This catalyst also outperforms other recently reported heterogeneous catalysts for ODS in similar systems. Both the new supports and the best catalyst, PMo/RPN-SiO₂, were characterized by elemental analysis, BET, SEM, multinuclear MAS NMR and FTIR.

Acknowledgements

Appendix A. Supplementary data

Supplementary material related to this article can be found, in the online version, at doi:https://doi.org/10.1016/j.apcatb.2018.03.005.

References

[1] Directive 2009/30/EC of the European Parliament and of the Council of 23 April 2009, http://www.eltis.org/sites/default/files/celex-32009l0030-en-txt.pdf (accessed 22 February 2018).
[2] I.V. Babich, J.A. Moulijn, Science and technology of novel processes for deep desulfurization of oil refinery streams, Fuel 82 (2003) 607–631.
[3] R. Prins, Hydrotreating, in: G. Ertl, H. Knözinger, F. Schüth, J. Weitkamp (Eds.), Handbook of Heterogeneous Catalysis, vol. 6, Wiley-VCH, 2008, pp. 2695–2718.
[4] A.W. Bhutto, R. Abro, S. Gao, T. Abbas, X. Chen, G. Yu, Oxidative desulfurization of fuel oils using ionic liquids: A review, J. Taiwan Inst. Chem. Eng. 62 (2016) 84–97.
[5] Z. Jiang, H. Lü, Y. Zhang, C. Li, Oxidative desulfurization of fuel oils, Chin. J. Catal. 32 (2011) 707–715.
[6] U. Domańska, K. Walczak, M. Królikowski, Extraction desulfurization process of fuels with ionic liquids, J. Chem. Thermodyn. 77 (2014) 40–45.
[7] J. Bu, G. Loh, C.G. Gwie, S. Dewiyanti, M. Tasrif, A. Borgna, Desulfurization of diesel fuels by selective adsorption on activated carbons: competitive adsorption of polycyclic aromatic sulfur heterocycles and polycyclic aromatic hydrocarbons, Chem. Eng. J. 166 (2011) 207–217.
[8] D. Boniek, D. Figueiredo, A.F.B. dos Santos, M.A. de Resende Stoianoff, Biodesulfurization: a mini review about the immediate search for the future technology, Clean Technol. Environ. Policy 17 (2014) 29–37.
[9] F.M. Collins, A.R. Lucy, C. Sharp, Oxidative desulphurisation of oils via hydrogen peroxide and heteropolyanion catalysis, J. Mol. Catal. A Chem. 117 (1997) 397–403.
[10] C. Komintarachat, W. Trakarnpruk, Oxidative desulfurization using polyoxometalates, Ind. Eng. Chem. Res. 45 (2006) 1853–1856.
[11] A.F. Shojaei, M.A. Rezvani, M.H. Loghmani, Comparative study on oxidation desulphurization of actual gas oil and model sulfur compounds with hydrogen peroxide promoted by formic acid: synthesis and characterization of vanadium containing polyoxometalate supported on anatase crushed nanoleaf, Fuel Process. Technol. 118 (2014) 1–6.
[12] A.E.S. Choi, S. Roces, N. Dugos, M.W. Wan, Oxidation by H₂O₂ of bezothiophene and dibenzothiophene over different polyoxometalate catalysts in the frame of ultrasound and mixing assisted oxidative desulfurization, Fuel 180 (2016) 127–136.
[13] M. Craven, R. Yahya, E.F. Kozhevnikova, C.M. Robertson, A. Steiner, I.V. Kozhevnikov, Alkylaminophosphazenes as efficient and tuneable phase-transfer agents for polyoxometalate-catalysed biphasic oxidation with hydrogen peroxide, ChemCatChem 8 (2016) 200–208.
[14] I.V. Kozhevnikov, Catalysts for Fine Chemical Synthesis: Catalysis by Polyoxometalates, Wiley, West Sussex, 2002.
[15] C. Venturello, J.C.J. Bart, M. Ricci, A new peroxotungsten heteropoly anion with special oxidizing properties: synthesis and structure of tetrahexylammonium tetra (diperoxotungsto)phosphate(3-), J. Mol. Catal. 32 (1985) 107–110.
[16] C. Venturello, M. Gambaro, A convenient catalytic method for the dihydroxylation of alkenes by hydrogen peroxide, Synthesis 4 (1989) 295–297.
[17] C. Venturello, R. D'Aloisio, Quaternary ammonium tetrakis(diperoxotungsto)phosphates(3-) as a new class of catalysts for efficient alkene epoxidation with hydrogen peroxide, J. Org. Chem. 53 (1988) 1553–1557.
[18] Y. Ishii, K. Yamawaki, T. Ura, H. Yamada, T. Yoshida, M. Ogawa, Hydrogen peroxide oxidation catalyzed by heteropoly acids combined with cetylpyridinium chloride: epoxidation of olefins and allylic alcohols, ketonization of alcohols and diols, and oxidative cleavage of 1,2-diols and olefins, J. Org. Chem. 53 (1988) 3587–3593.
[19] R. Yahya, M. Craven, E.F. Kozhevnikova, A. Steiner, P. Samunual, I.V. Kozhevnikov, D.E. Bergbreiter, Polyisobutylene oligomer-bound polyoxometalates as efficient and recyclable catalysts for biphasic oxidations with hydrogen peroxide, Catal. Sci. Technol. 5 (2015) 818–821.
[20] H.R. Allcock, Recent advances in phosphazene (phosphonitrilic) chemistry, Chem. Rev. 72 (1972) 315–356.
[21] A.K. Andrianov (Ed.), Supramolecular Structures of Cyclotriphosphazenes, Polyphosphazenes for Biomedical Applications, John Wiley & Sons, Inc., 2009.
[22] M. Craven, R. Yahya, E.F. Kozhevnikova, R. Boomishankar, C.M. Robertson, A. Steiner, I.V. Kozhevnikov, Novel polyoxometalate-phosphazene aggregates and their use as catalysts for biphasic oxidations with hydrogen peroxide, Chem. Commun. 49 (2013) 349–351.
[23] M. Zhang, W. Zhu, H. Li, M. Li, S. Yin, Y. Li, Y. Wei, H. Li, Facile fabrication of molybdenum-containing ordered mesoporous silica induced deep desulfurization in fuel, Colloids Surf. A. 504 (2016) 174–181.
[24] J. Zhang, A. Wang, Y. Wang, H. Wang, J. Gui, Heterogeneous oxidative desulfurization of diesel oil by hydrogen peroxide: catalysis of an amphipathic hybrid material supported on SiO₂, Chem. Eng. J. 245 (2014) 65–70.
[25] J.M. Fraile, C. Gil, J.A. Mayoral, B. Muel, L. Roldán, E. Vispe, S. Calderón, F. Puente, Heterogeneous titanium catalysts for oxidation of dibenzothiophene in hydrocarbon solutions with hydrogen peroxide: on the road to oxidative desulfurization, Appl. Catal. B Environ. 180 (2016) 680–686.
[26] M. Vigolo, S. Borsacchi, A. Soraru, M. Geppi, B.M. Smarsly, P. Dolcet, S. Rizzato, M. Carraro, S. Gross, Engineering of oxoclusters-reinforced polymeric materials with application as heterogeneous oxydesulfurization catalysts, Appl. Catal. B Environ. 182 (2016) 636–644.
[27] D. Julião, A.C. Gomes, M. Pillinger, R. Valença, J.C. Ribeiro, B. de Castro, I.S. Gonçalves, L. Cunha Silva, S.S. Balula, Zinc-substituted polyoxotungstate@amino-MIL-101(Al) – an efficient catalyst for the sustainable desulfurization of model and real diesels, Eur. J. Inorg. Chem. 2016 (2016) 5114–5122.
[28] B.M. Fung, A.K. Khitrin, K. Ermolaev, An improved broadband decoupling sequence for liquid crystals and solids, J. Magn. Reson. 142 (2000) 97–101.
[29] C.R. Morcombe, K.W. Zilm, Chemical shift referencing in MAS solid state NMR, J. Magn. Reson. 162 (2003) 479–486.
[30] E. Brendler, T. Heine, A.F. Hill, J. Wagler, A pentacoordinate chlorotrimethylsilane derivative: A very polar snapshot of a nucleophilic substitution and its influence on ²⁹Si solid state NMR properties, Z. Anorg. Allg. Chem. 635 (2009) 1300–1305.
[31] J. Ledger, R. Boomishankar, A. Steiner, Aqueous chemistry of chlorocyclophosphazenes: phosphates {PO(2)}, phosphamides {P(O)NHR}, and the first phosphites {PHO} and pyrophosphates {(PO)(2)O} of these heterocycles, Inorg. Chem. 49 (2010) 3896–3904.
[32] M. Kruk, M. Jaroniec, Gas adsorption characterization of ordered organic-inorganic nanocomposite materials, Chem. Mater. 13 (2001) 3169–3183.
[33] K.S.W. Sing, D.H. Everett, R.A.W. Haul, L. Moscou, R.A. Pierotti, J. Rouquérol, T. Siemieniewska, Reporting physisorption data for gas/solid systems with special reference to the determination of surface area and porosity, Pure Appl. Chem. 57 (1985) 603–619.
[34] S.S. Lim, G.I. Park, I.K. Song, W.Y. Lee, Heteropolyacid (HPA)-polymer composite films as catalytic materials for heterogeneous reactions, J. Mol. Catal. A Chem. 182 (2002) 175–183.
[35] Y. Kim, W. Lee, Characterization of the catalytic heteropoly compounds using solid-state NMR, J. Korean Magn. Reson. Soc. 1 (1997) 45–58.
[36] C. Rocchiccioli-Deltcheff, M. Fournier, R. Franck, R. Thouvenot, Evidence for anion-anion interactions in molybdenum(VI) and tungsten(VI) compounds related to the Keggin structure, Inorg. Chem. 22 (1983) 207–216.
[37] I.V. Kozhevnikov, Catalysis by heteropoly acids and multicomponent polyoxometalates in liquid-phase reactions, Chem. Rev. 98 (1998) 171–198.
[38] D. Feakins, Structure and basicity. Part II. The basicity of fully aminolysed

cyclotriphosphazatrienes and cyclotetraphosphazatetraenes in nitrobenzene and water, J. Chem. Soc. (1964) 4464–4471.

[39] X. Jiang, H. Li, W. Zhu, L. He, H. Shu, J. Lu, Deep desulfurization of fuels catalyzed by surfactant-type decatungstates using H_2O_2 as oxidant, Fuel 88 (2009) 431–436.

[40] J. Zhang, A. Wang, X. Li, X. Ma, Oxidative desulfurization of dibenzothiophene and diesel over $[Bmim]_3PMo_{12}O_{40}$, J. Catal. 279 (2011) 269–275.